Sustainable Energy & Fuels

ROYAL SOCIETY OF CHEMISTRY

PAPER

View Article Online
View Journal

Cite this: DOI: 10.1039/d5se01101a

Integration of formic acid dehydrogenation with electrochemical pumping for the generation of clean hydrogen

Fabian Ketter, [a] Shwetambara Jha, [a] Sonja D. Mürtz [a] and Regina Palkovits *[abc]

Received 14th August 2025
Accepted 16th September 2025

DOI: 10.1039/d5se01101a

rsc.li/sustainable-energy

Hydrogen purification is a crucial challenge for the efficient use of hydrogen as a sustainable energy carrier. However, systems combining the formation of hydrogen from easily transportable liquid organic carriers with purification after release are rarely reported. Here, we present an integrated system combining formic acid dehydrogenation (FADH) and electrochemical hydrogen pumping (EHP) for hydrogen purification. The $[RuCl_2(p\text{-cymene})]_2$-catalysed dehydrogenation of formic acid generated stable H_2-CO_2 mixtures with ratios of 1 : 1 and 2 : 1. Small-scale EHP tests demonstrated that a supported PdPt catalyst exhibits high hydrogen oxidation reaction (HOR) activity and enhanced CO tolerance compared to a Pt benchmark catalyst. This integrated system offers a promising approach for hydrogen purification with potential applications in fuel cells and hydrogen storage systems.

Introduction

Due to increasing global energy demand, coupled with challenges such as rising temperatures and extreme weather events caused by greenhouse gas emissions, significant environmental and economic pressures have developed worldwide. Hence, current research efforts focus on the advancement of sustainable methods for energy production and storage.[1–4]

In this context, hydrogen is considered a promising energy carrier due to its potential to provide secure and uninterrupted energy supply and its widespread use in chemical synthesis.[5,6] Fuel cells efficiently convert chemical energy into electrical energy, while water is produced as the main product.[7] When hydrogen is produced through water electrolysis using renewable energy sources, green hydrogen offers a carbon-neutral alternative to conventional fossil fuels. However, despite these advantages, approximately 80% of hydrogen is still produced by methane steam reforming (SMR), which generates CO_2 as a by-product (grey hydrogen).[5,8] Critical challenges for the efficient usage of hydrogen are storage and transport. With commonly applied storage techniques at high pressures (350–700 bar) or at low temperatures in the liquid state (about −253 °C), comparably low volumetric energy densities of 3–9 MJ L^{-1} are achieved.[9] In contrast, gasoline offers a volumetric energy density of 34 MJ L^{-1}.[10]

Liquid organic hydrogen carriers (LOHCs), such as formic acid, offer an alternative with higher volumetric energy density under ambient conditions. However, LOHC-based hydrogen production often generates impure hydrogen streams containing CO_2, CO, CH_4, and other gases. Thus, subsequent purification remains essential for efficient hydrogen utilisation.[11]

State-of-the-art purification methods include pressure swing adsorption (PSA) and membrane-based techniques.[12–14] A promising and cost-effective alternative as shown by various techno-economic analyses offers electrochemical hydrogen pumping (EHP).[13–16]

Fig. 1 illustrates the currently accepted vision of a hydrogen economy and possible roles of liquid organic hydrogen carriers and EHPs within the value chain. EHPs utilise proton-exchange membranes (PEMs) to separate impurities during the hydrogen oxidation reaction (HOR) at the anode, while simultaneously generating pressurised hydrogen in the cathode compartment during the hydrogen evolution reaction (HER). For the occurring reactions, platinum-based catalyst systems are commonly used due to their high activity.[3,17]

Research efforts for electrochemical hydrogen pumps strongly focus on improving the efficiency of such systems. Thus, the reduction of activation-, mass transport-, and ohmic overpotentials is extensively studied.[14] A schematic setup of an EHP is presented in Fig. 2.

A critical challenge towards the efficient use of EHPs presents poisoning of the anode catalyst by impurities like CO_2 and CO in the feed stream. To mitigate these effects, alloying

[a]Chair of Heterogeneous Catalysis and Chemical Technology, Institute for Technical and Macromolecular Chemistry, RWTH Aachen University, Worringerweg 2, 52074 Aachen, Germany. E-mail: palkovits@itmc.rwth-aachen.de

[b]Institute for a Sustainable Hydrogen Economy (INW-2), Forschungszentrum Jülich GmbH, Marie-Curie Straße 5, 52428 Jülich, Germany. E-mail: r.palkovits@fz-juelich.de

[c]Max-Planck-Institut for Chemical Energy Conversion, Stiftstr. 34-36, 42470 Mülheim a. d. Ruhr, Germany

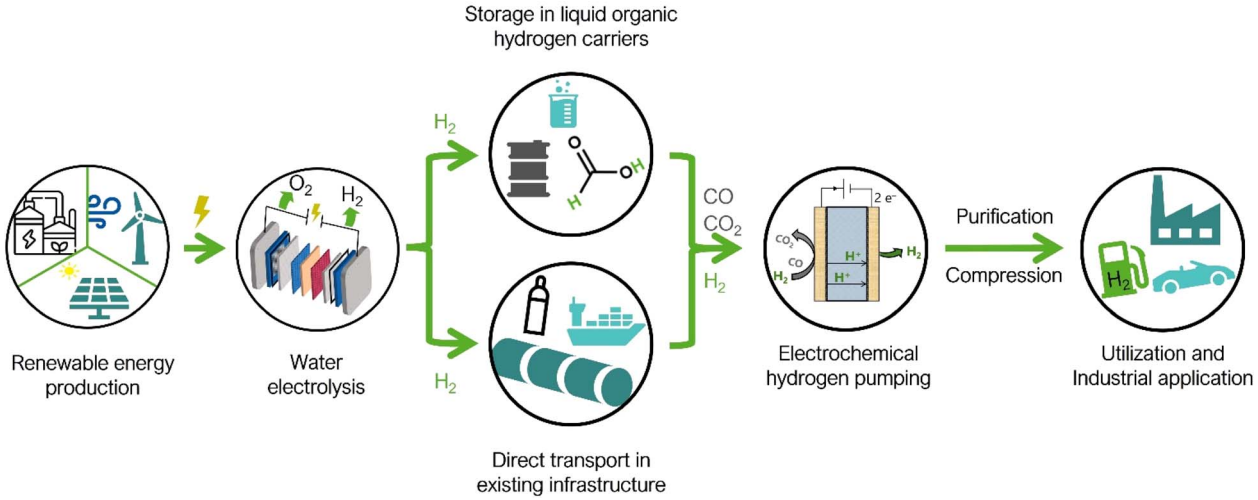

Fig. 1 Schematic overview of a hydrogen economy. Electricity from renewable energy sources is used to produce hydrogen through water electrolysis. The generated hydrogen can either be stored in liquid organic hydrogen carriers or be directly transported in existing infrastructure. Electrochemical hydrogen pumping allows for purification and simultaneous compression at the location of utilization or industrial application.

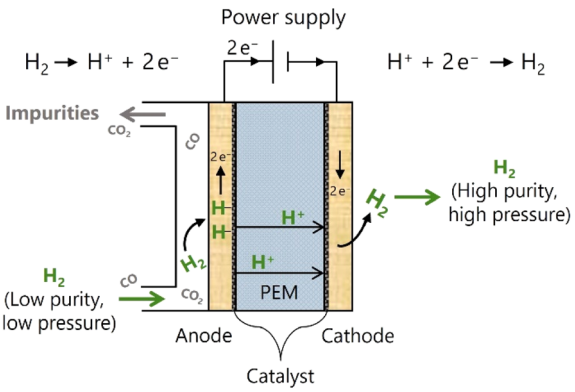

Fig. 2 Schematic setup of an electrochemical hydrogen pump. Hydrogen is oxidised to protons at the anode (left) and transported through a proton-exchange membrane (PEM). At the cathode (right), the protons are reduced back to high-purity hydrogen.

platinum with other metals like palladium has been shown to lead to increased CO tolerance due to enhanced chemisorption of hydroxyl groups that promote CO oxidation.[17,18] The mechanism for CO electrooxidation is explained in more detail in Fig. S1.[19]

Although considerable research efforts focus on the optimisation of hydrogen supply from LOHCs[20–23] and electrochemical hydrogen pumping[15,24–26] individually, barely any studies have explored integrated systems.[27] In previous studies, Wu *et al.* and Liu *et al.* used EHPs for thermo-electrochemical dehydrogenations of methanol[28,29] and ethanol[30] with pure feed streams. Mrusek *et al.* focused on LOHC systems that deliver relatively pure hydrogen.[27] However, in practical applications, hydrogen generated from LOHC dehydrogenation often contains impurities such as CO and CO_2, which can negatively affect system performance.

Herein, we address this gap by presenting an integrated system that combines LOHC-derived hydrogen generation with controlled impurities and EHPs. By post-processing the gas generated from LOHC decomposition, the system's performance is examined under varying conditions. In this way, this study provides insights into the practicability of combining LOHC decomposition with EHP under relevant conditions.

To achieve this, we optimise the catalytic dehydrogenation of formic acid to provide a stable gas stream with controlled amounts of impurities, which is then fed into an electrochemical hydrogen pumping cell. In the electrochemical cell, palladium-platinum catalysts supported on reduced graphene oxide (PdPt@rGO) are used for increased tolerance against catalyst poisons such as CO and CO_2, maintaining high hydrogen oxidation activity under challenging conditions.[17,18] Owing to their oxophilicity, the addition of palladium and the use of reduced graphene oxide (rGO) as support facilitate the oxidation of catalyst poisons such as CO. Furthermore, compared to other carbon-based supports, rGO increases the catalyst's polarity, improving wetting and electrochemical connectivity to the sulfuric acid electrolyte. This can lead to enhanced catalyst performance. The catalysts are synthesised by a facile hydrothermal method and characterized by means of X-ray diffraction (XRD), inductively coupled plasma-optical emission spectroscopy (ICP-OES), and X-ray photoelectron spectroscopy (XPS).

As far as our knowledge, this study for the first time explores integrated systems of LOHC decomposition generating impure hydrogen streams and electrochemical hydrogen pumping in a straightforward and simple setup.

Experimental

Formic acid dehydrogenation

For a typical formic acid dehydrogenation (FADH) experiment, sodium formate (2.955 g, 45.6 mmol, ≥99%, Carl Roth) and

$[RuCl_2(p\text{-cymene})]_2$ (91.8 mg, 0.15 mmol, Sigma-Aldrich) were dissolved in aqueous formic acid solution (700 g L^{-1}, 114 mmol, 7.5 mL, ≥99%, Th. Geyer). The reaction was initiated at 110 °C, and the gases were analysed with on-line mass spectrometry (MS, Pfeiffer GSD 350 OmniStar) using a nitrogen stream of 20 mL min^{-1} as carrier gas. The calculation of the produced amount of H_2- and CO_2 gas streams is shown in eqn (S1) and (S2) in the SI.

For the experiments involving a gas washing step, the produced gas was passed through a gas washing bottle containing a sodium phosphate solution (0.75 M, ≥98%, 250 mL, pH = 12, Sigma-Aldrich) as washing medium.

Catalyst synthesis

Hydrogen oxidation catalysts were synthesised by a simple hydrothermal procedure. First, exfoliation of graphene oxide (200 mg, 4–10% edge-oxidized, Sigma-Aldrich) was conducted in deionized water (15 mL) for 15 minutes with the aid of ultrasonication. Subsequently, $PtCl_2$ (Pt@rGO: 17 mg, 64 μmol/PdPt@rGO: 5.9 mg, 22 μmol, ≥99.9%, Sigma-Aldrich) and $PdCl_2$ (PdPt@rGO: 13.7 mg, 78 μmol, ≥99.9%, Sigma-Aldrich) were added and dispersed for another 10 minutes through ultrasonication. The prepared dispersion was transferred to a Teflon-lined autoclave and sodium borohydride (Pt@rGO: 13.3 mg, 0.35 mmol/PdPt@rGO: 21.6 mg, 0.57 mmol, Sigma-Aldrich) was slowly added. The dispersion was then allowed to react at 200 °C for 12 h under autogenic pressure. Subsequently, the product was centrifuged, washed with water. and dried in a drying oven at 80 °C for 24 h. The corresponding reaction for catalyst synthesis is shown in Scheme 1, where (r)GO represents (reduced) graphene oxide.

Physical catalyst characteriation

X-ray diffraction measurements were carried out on a D2 Phaser diffractometer from Bruker® with an acceleration voltage of 30 kV and Cu-Kα radiation in a 2 θ range of 6–90° in 0.02° steps. The average crystallite size was determined using the Scherrer Equation (eqn (S3) in the SI) at the (220) reflection of the synthesised catalysts. The shape factor was assumed to be 0.9 in this work.[31]

X-ray photoelectron spectroscopy (XPS) measurements were carried out on an AXIS Supra$^+$ spectrometer from Kratos Analytical Ltd with a monochromatic Al-Kα X-ray source operated at 25 W. The sample holder was covered with non-conductive tape to mitigate charging effects and the powder samples were applied on top of the holder, which was covered with double-sided carbon tape. Survey spectra were acquired in a binding energy (BE) range of 1400–0 eV with a step size of 1 eV and a pass energy of 160 eV. Large area region scans were measured with a step size of 0.1 eV, a pass energy of 20 eV, 20 sweeps per region and a scan time of 60 s per sweep. During all measurements, the base pressure in the analysis chamber was below 8.4×10^{-9} mbar. Data acquisition was conducted with aid of the ESCApe™ software.[32] Data analysis and fitting were performed with CasaXPS.[33] For the correction of charging effects, binding energies were referenced to the C 1s BE of adventitious sp^3 carbon at 284.8 eV.[34]

Inductively coupled plasma-optical emission spectroscopy (ICP-OES) was used for the determination of the metal loading. The catalysts were dissolved in aqua regia with the aid of a microwave. The obtained catalyst solution was analysed by ICP-OES on a Spectroblue device from SPECTRO® Analytical Instruments GmbH.

$$PtCl_2 + GO + 6\,H_2O + 2\,NaBH_4 \rightarrow Pt@rGO + 3\,H_2 + 2\,B(OH)_3 + 2\,NaCl$$

Scheme 1 Reaction equation for the hydrothermal synthesis of Pt@rGO catalysts. The reduction of $PdCl_2$ is expected to proceed in the same way.

Electrochemical catalyst characterisation

The applied or recorded potentials E_{pstat} were 85% iR-corrected and referenced to the RHE to obtain E_{RHE} by adding the constant potential of the Ag/AgCl (3 M KCl) RE measured as 0.244 V *vs.* RHE against a hydrogen RE (HydroFlex, Gaskatel) according to eqn (1), where i represents the applied or recorded current and R_U denotes the uncompensated resistance determined by electrochemical impedance spectroscopy.[35]

$$E_{RHE} = E_{pstat} + 0.244\ V - i \times R_U \quad (1)$$

Electrochemical measurements were performed according to the following protocol:

1. Determination of the open circuit potential (OCP) for 900 s during which the electrolyte is saturatedwith the respective gas.
2. Electrochemical impedance spectroscopy (PEIS) at the OCP with a perturbation root mean square voltage of 10 mV in a frequency range of 100 kHz to 1 Hz.
3. Recording of 5 CVs in a potential range of −0.06 V to 1.44 V *vs.* Ag/AgCl with a scan rate of 50 mV s^{-1}.
4. Recording of one LSV in a potential range of −0.54–0.74 V *vs.* RHE at a scan rate of 5 mV s^{-1}.
5. Chronoamperometry at a potential of 0.74 V *vs.* RHE for 1200 s.

Results and discussion

Formic acid dehydrogenation

In a first step, the controlled release of hydrogen by formic acid dehydrogenation (FADH) was optimised to adequately supply the electrochemical hydrogen pumping (EHP) cell in this work. A hydrogen flow rate of 30 mL min^{-1} over at least 30 min is assumed to be sufficient for electrochemical measurements in a small-scale EHP cell.

FADH was performed with the homogeneous Ru catalyst $[RuCl_2(p\text{-cymene})]_2$ and a sodium formate base as proposed by Guan *et al.*[21] The homogeneous catalyst $[RuCl_2(p\text{-cymene})]_2$ was selected as FADH catalyst as it is a commercially available, affordable precursor that has been widely used for formic acid dehydrogenation, showing good activity while being stable under ambient storage and handling conditions.[21,36]

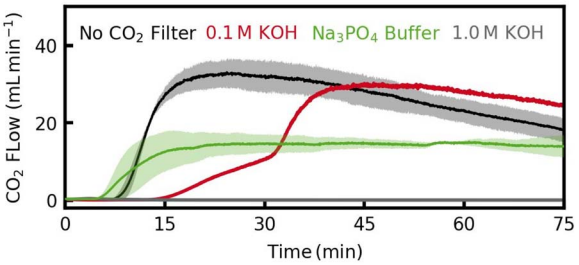

Fig. 3 CO_2-flow of the formic acid dehydrogenation under optimised conditions with- and without post-processing.

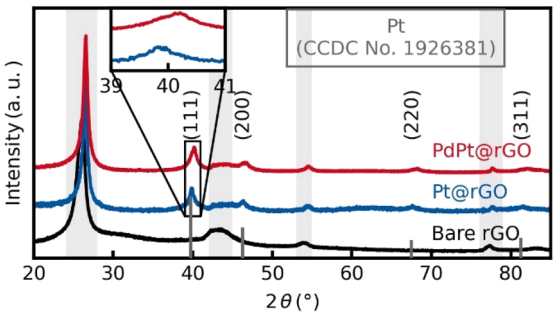

Fig. 4 Powder X-ray diffraction patterns of the reduced graphene oxide (rGO) support (black), Pt@rGO (blue) and PdPt@rGO (red).

While long-term stability of such catalysts is limited under reaction conditions, advanced ligand engineering and immobilization of the used precursor could further improve both activity and durability, rendering the catalyst suitable for industrial application.[20,37] The dehydrogenation setup and the structure of the employed catalyst are shown in Fig. S2. The reaction conditions were varied to temperatures up to 110 °C (see Fig. S3 and S4). Gas chromatography analyses showed that the CO concentration in the product gas was below the detection limit of 10 ppm, indicating high catalyst selectivity towards the dehydrogenation reaction and suppression of competing dehydration.

To obtain a H_2-to-CO_2 ratio that more closely resembles the composition of typical industrial reformate gas streams with a CO_2-content of 20–25%, the gas stream from FADH was post-processed using a simple gas washing procedure with different washing media.[38] After an induction period of approximately 10–20 min, the detected CO_2 flow remains stable at approximately 15 mL min^{-1} using a sodium phosphate buffer (Fig. 3).

After the reaction, the pH of the sodium phosphate buffer was 10.6 in all measurements. Contrary, experiments with a 1 M KOH washing medium led to complete removal of CO_2 from the gas stream. The CO_2 filtration capacity of 0.1 M KOH varies throughout the reaction, possibly due to a decrease in pH with increasing CO_2 absorption. Thus, the sodium phosphate buffer performed best and was used in further experiments.

Physical catalyst characterisation

The synthesised HOR catalysts were characterised by powder X-ray diffraction (XRD) and inductively coupled plasma-optical emission spectroscopy (ICP-OES). The XRD patterns show the characteristic reflections of bare reduced graphene oxide (rGO), indicated by the shaded areas in Fig. 4.[39] Additional reflections are observed at 2θ values of 39–40°, 46–47°, 67–68°, 81–82° and 83–84°, corresponding to the formation of Pt or PdPt particles in the cubic crystal structure on the rGO support, respectively. For the PdPt@rGO catalyst (red line in Fig. 4), the characteristic reflections for the metal particles are shifted to higher 2θ values.[40] This can be attributed to the presence of palladium in the catalyst leading to a decreased lattice spacing due to the lower spatial requirement of palladium compared to platinum.[40]

The application of Scherrer equation to the reflection of the (220) plane of the Pt- and PdPt nanoparticles revealed average crystallite sizes 14 and 21 nm, respectively. ICP-OES analyses further confirmed the successful deposition of platinum and palladium species on reduced graphene oxide. The Pt@rGO catalyst showed a platinum loading of 38.5(5) mg g^{-1}, while the PdPt@rGO catalyst showed a Pt loading of 15.1(2) mg g^{-1} and a Pd loading of 29.7(4) mg g^{-1}. Thus, the total metal content of both catalysts is comparable under the applied synthesis conditions.

Electrochemical catalyst characterization and system integration

To investigate the electrochemical performance of the catalysts, electrochemical measurements were carried out in an EHP cell. Additionally, the composition of the gas stream from the dehydrogenation was simultaneously investigated with on-line mass spectrometry. Fig. 5 shows the time evolution of the mass spectrometry signals for hydrogen ($m/z = 2$), carbon dioxide ($m/z = 44$) and nitrogen ($m/z = 14$) after the start of the

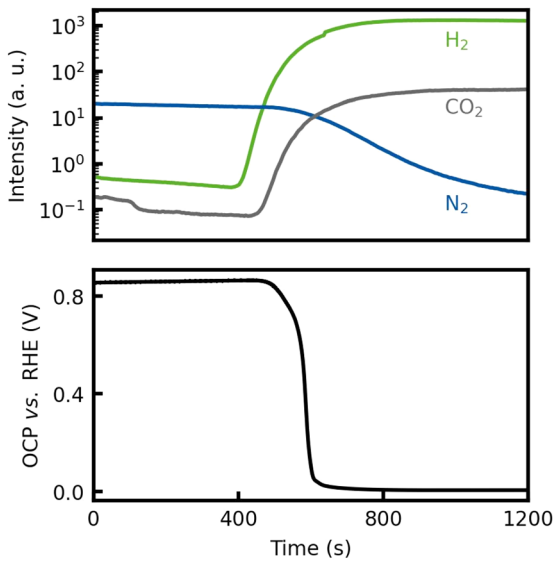

Fig. 5 Time evolution of the H_2 and CO_2 generation from formic acid dehydrogenation (top) and the open circuit potential (OCP) of the electrochemical cell fed with the gas mixture from formic acid dehydrogenation (bottom).

reaction as well as the open circuit potential of the working electrode in the EHP cell for the PdPt@rGO catalyst during the saturation of the electrolyte. Further information on the hydrogen yield of the dehydrogenation reaction and experimental details on the employed setup are presented in Fig. S5 and S6, respectively.

After an induction period of approximately 600 s, during which the generated gases displace the air in the apparatus, both hydrogen and carbon dioxide reach the mass spectrometer and the signal intensities for those gases stabilise at high levels. Conversely, the signal intensity of nitrogen decreases, showing its displacement from the apparatus. When the produced hydrogen reaches the EHP cell after approximately 600 s, the open circuit potential (OCP) of the working electrode sharply drops from approximately 0.8 V *vs.* RHE to the equilibrium value in hydrogen-saturated electrolyte of approximately 0 V *vs.* RHE. This indicates that the conditions required for the HOR are established when hydrogen dissolves in the electrolyte within the anode compartment. Under open-circuit conditions, the working electrode potential decreases to a value where the HOR does not proceed.

To investigate the performance of the synthesized catalysts in the HOR, cyclic voltammetry was performed. Fig. 6 shows cyclic voltammograms (CVs) recorded in electrolyte saturated with nitrogen, hydrogen and the gas stream from formic acid dehydrogenation after the gas washing process for the PdPt@rGO catalyst.

In the CV recorded in nitrogen-saturated electrolyte, the expected features for platinum-based catalysts are observed. This includes the HER onset at potentials below 0 V *vs.* RHE, the underpotential hydrogen deposition signals in the potential region between 0 V and 0.2 V *vs.* RHE and the Pt oxidation signals at 0.5–0.7 V *vs.* RHE.[41] No significant currents indicating other faradaic processes are observed in the cyclic voltammograms besides these characteristic signals.

In hydrogen-saturated electrolyte, higher currents are observed across the investigated potential range. This indicates the occurrence of the hydrogen oxidation reaction. These observations also apply when the formic acid-derived gas is used as a feed. In these experiments, lower current densities are reached compared to the experiments with pure hydrogen. Possibly, this is owed to the hydrogen dilution with CO_2, leading to a decreased hydrogen concentration in the electrolyte. In the experiments with hydrogen and the formic acid-derived gas mixture, the highest current densities are observed at potentials of approximately 1.2 V *vs.* RHE. Presumably, this can be attributed to increased formation of platinum oxides that may reduce the activity towards HOR. Similar findings were reported in earlier studies with rotating disk electrodes.[42,43] To further evaluate catalyst performance in HOR, chronoamperometry was carried out at 0.74 V *vs.* RHE. These results are presented in Fig. 7.

For both catalysts, the highest current densities are observed in hydrogen-saturated electrolyte, while no significant currents were measured in nitrogen-saturated electrolyte. The catalyst's stability was further examined by chronoamperometry in hydrogen saturated electrolyte over 12 h, during which only minimal activity loss was observed, indicating a high stability of the catalyst under reaction conditions (see Fig. S7). In experiments with the formic acid derived gas mixtures, reduced current densities are observed compared to those obtained with pure hydrogen. This decrease can be attributed to the presence of carbon dioxide in this gas stream, which dilutes hydrogen and, thus, may lead to decreased hydrogen concentration in the electrolyte. Additionally, trace amounts of carbon monoxide from the catalytic dehydrogenation could be present in the gas stream and lead to minor catalyst poisoning, although they were not detected in the gas chromatography analyses. When the gas stream is not post-processed, the dilution effect increases, leading to a further decrease in current density. However, with all three FADH-derived gas streams, the hydrogen oxidation reaction is performed effectively, demonstrating the successful integration of both systems in a simple and straightforward setup. These results highlight the possibility of employing gas streams from formic acid dehydrogenation or related liquid organic hydrogen carrier systems for electrochemical hydrogen pumping.

Experiments with impure hydrogen as feed gas for the electrochemical cell showed reduced current densities compared to the experiments with pure hydrogen. This effect can be attributed to CO-induced catalyst poisoning. A comparison between the Pt@rGO and the PdPt@rGO catalysts emphasises that, despite the lower Pt-loading in the PdPt catalyst, the Pt@rGO catalyst exhibits a similar average current density of 1.9 mA cm^{-2} compared to PdPt@rGO. This may indicate a higher tolerance against CO poisoning for the PdPt@rGO catalyst.

To support this hypothesis, cyclic voltammetry was conducted using a gas mixture containing hydrogen with 1000 ppm CO and 1000 ppm CO_2. Representative CVs for both catalysts are shown in Fig. 8.

Both cyclic voltammograms exhibit the characteristic broad Pt-oxidation signal at a potential of approximately 0.6 V *vs.* RHE. However, the characteristic signals for underpotential hydrogen deposition are only present in the PdPt@rGO catalyst. This can

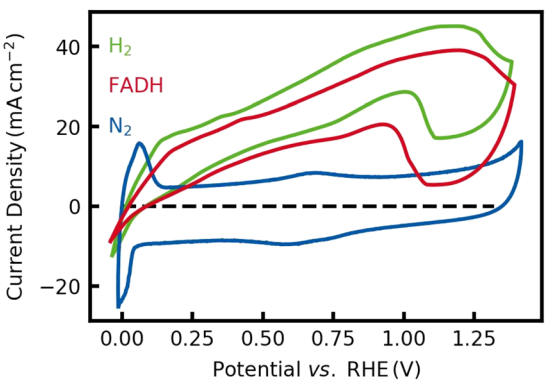

Fig. 6 Cyclic voltammograms recorded in electrolyte saturated with nitrogen (blue), hydrogen (green) and the gas stream from formic acid dehydrogenation (red) for PdPt@rGO. CVs were recorded at a scan rate of 50 mV s^{-1}.

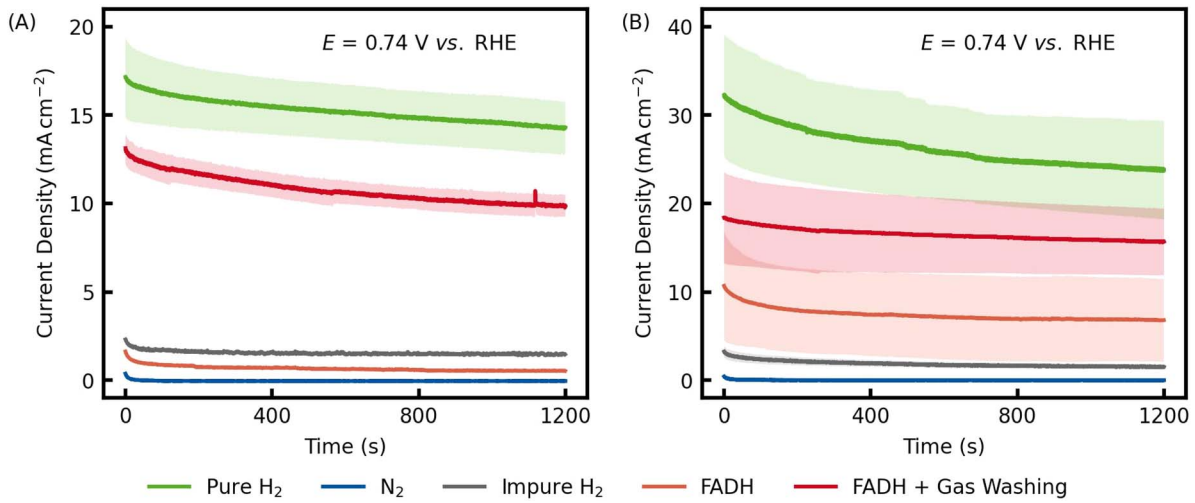

Fig. 7 Chronoamperometry at 0.74 V *vs.* RHE for (A) the Pt@rGO benchmark catalyst and (B) the PdPt@rGO catalyst in electrolyte saturated with nitrogen (blue), hydrogen (green), hydrogen with 1000 ppm CO and 1000 ppm CO_2 (gray) the gas mixture from formic acid dehydrogenation (light red, gas composition: approx. 50 vol% H_2, 50 kratosvol% CO_2) and the post-processed gas mixture from formic acid dehydrogenation (red, gas composition: approx. 66 vol% H_2, 34 vol% CO_2). Shaded areas indicate the standard deviation across at least two independent measurements.

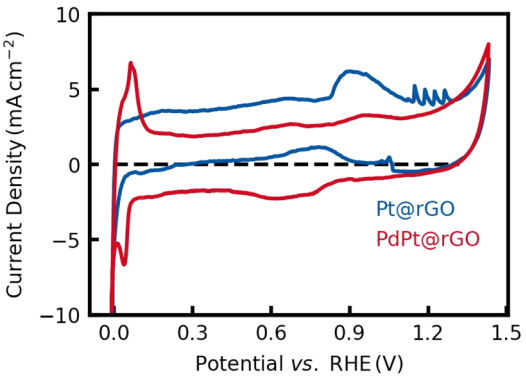

Fig. 8 Representative cyclic voltammograms in sulphuric acid electrolyte saturated with hydrogen containing 1000 ppm CO and 1000 ppm CO_2 of the Pt@rGO (blue) and the PdPt@rGO (red) catalyst. Cyclic voltammograms were recorded at a scan rate of 10 mV s^{-1}.

be attributed to the blocking of Pt-sites with CO on the Pt@rGO catalyst. In the PdPt@rGO catalyst, underpotential hydrogen deposition is still observed. Possibly, this can be assigned to hydrogen deposition on the Pd-sites that are only poisoned to a lower extent compared to the Pt sites.

In addition to these signals, additional broad peaks are observed at onset potentials of approximately 0.82 V *vs.* RHE. These signals can be attributed to the CO-oxidation to CO_2, liberating the respective catalytic site for hydrogen oxidation. The lower oxidation current with the PdPt@rGO catalyst may further support a greater tolerance against carbon monoxide indicating that less platinum is poisoned with CO compared to the Pt@rGO catalyst. For the Pt@rGO system, an oscillating current is measured at potentials above the CO-oxidation potential. This behavior is likely due to the mechanism of CO-poisoning and liberation of CO sites and has previously been reported in both experimental[44] and theoretical[45] studies.

To further examine the enhanced CO-tolerance, XPS studies were performed to investigate the Pt and Pd surface oxidation states. Fig. 9 shows large area region scans of the Pt 4f (binding energy of approx. 75 eV) and Pd 3d (binding energy of approx. 340 eV) regions for the two synthesised catalysts.[46]

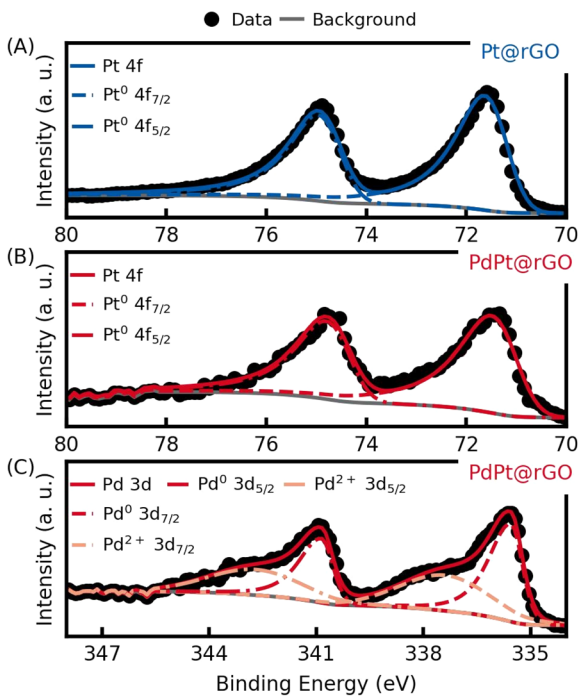

Fig. 9 Large area region scans the Pt 4f region of the (A) Pt@rGO and (B) PdPt@rGO catalyst and (C) the Pd 3d region of the PdPt@rGO catalyst.

All scans show the expected spin–orbit splitting for both platinum and palladium species. The deconvolutions of these scans reveal the absence of oxidised platinum species in both catalysts. In the PdPt@rGO catalyst, Pd is present in oxidation states 0 (56%) and +2 (44%). The presence of oxidised Pd species supports the hypothesis that Pd facilitates the chemisorption of hydroxyl species, which are crucial for CO oxidation and the liberation of catalytic sites for hydrogen oxidation (see Fig. S1 for details). These findings are in line with various studies in literature reporting enhanced OH chemisorption by alloying palladium and platinum.[17–19,47] The corresponding XPS survey scans of the catalysts are presented in Fig. S8.[13,14]

Conclusions

In this study, we present an integrated system including a LOHC decomposition unit together with an electrochemical hydrogen pump. The generation of hydrogen with controlled impurities was successfully performed through the $[RuCl_2(p\text{-cymene})]_2$-catalysed dehydrogenation of formic acid. The reaction conditions and post-processing of the produced gas were optimized to generate stable streams of approximately 45 mL min^{-1} with H_2-to-CO_2 ratios of 1 : 1 and 2 : 1, respectively.

Graphene oxide supported platinum (Pt@rGO) and palladium-platinum (PdPt@rGO) electrocatalysts were synthesised with a facile hydrothermal method and characterised for their physicochemical properties and catalytic activity in the HOR. Inductively coupled plasma-optical emission spectroscopy (ICP-OES) and X-ray diffraction (XRD) experiments confirmed the presence of 4–4.5 wt% Pt or PdPt particles on the catalysts. X-ray photoelectron spectroscopy showed that the surface of the PdPt@rGO catalyst contains Pt^0, Pd^0 and Pd^{2+} species, which may contribute to the increased CO tolerance of this catalyst compared to Pt@rGO that primarily contains elemental platinum. Cyclic voltammetry and chronoamperometry experiments in sulphuric acid saturated with nitrogen, pure hydrogen and the gas streams produced through formic acid dehydrogenation proved the high activity of the synthesised catalysts in the HOR and further suggest a higher CO-tolerance of the PdPt@rGO catalyst compared to the Pt@rGO system. Furthermore, the successful integration of the formic acid dehydrogenation with electrochemical pumping in a combined system with both catalysts was demonstrated. This integrated approach marks a significant step towards a scalable hydrogen economy by enabling the purification of impure LOHC-derived hydrogen streams for efficient large-scale energy storage and fuel cell applications.

Author contributions

Fabian Ketter: investigation, data curation, methodology, visualization and writing – original draft. Shwetambara Jha: conceptualization, methodology, funding acquisition and writing – review and editing. Sonja D. Mürtz: methodology and writing – review and editing. Regina Palkovits: conceptualization, methodology, funding acquisition and writing – review and editing.

Conflicts of interest

There are no conflicts to declare.

Data availability

Data for this article, including raw data files for the presented figures and metadata, are available at **https://doi.org/10.5281/zenodo.16636114**.

Further data and information supporting the findings of this article have been included in the supplementary information (SI). See DOI: **https://doi.org/10.1039/d5se01101a**.

Acknowledgements

We would like to thank Noah Avraham-Radermacher for XRD analyses, Heike Bergstein for ICP-OES measurements and Nick Hausen and Matthias Urban for assistance with the acquisition and interpretation of XPS data. Financial support from Deutsche Forschungsgemeinschaft (DFG) within the project (ID: 516338899) IRTG 2983 Hy-Potential is gratefully acknowledged. This work was also funded by the Federal Ministry of Research, Technology and Space within Hydrogen Cluster4Future (HylnnoSep2 - FKZ: 03ZU2115EA). The authors acknowledge the funding by the German Federal Ministry of Research, Technology and Space (BMFTR) and the Ministry of Economic Affairs, Industry, Climate Action and Energy of the State of North Rhine-Westphalia through the project HC-H2.

References

1 M. J. B. Kabeyi and O. A. Olanrewaju, *Front. Energy Res.*, 2022, **9**, 743114.
2 J. Hu, C. Zhang, X. Meng, H. Lin, C. Hu, X. Long and S. Yang, *J. Mater. Chem. A*, 2017, **5**, 5995–6012.
3 H. A. Gasteiger and N. M. Markovíc, *Science*, 2009, **324**, 48–49.
4 N. M. Kubo, F. Ketter, S. Palkovits and R. Palkovits, *ChemElectroChem*, 2024, **11**, e202300460.
5 L. García, in *Compendium of Hydrogen Energy*, ed. R. K. Gupta, A. Basile and T. N. Veziroglu, Elsevier, Oxford, 2015, ch. 4, pp. 83–107.
6 M. A. Rosen and S. Koohi-Fayegh, *Energy, Ecol. Environ.*, 2016, **1**, 10–29.
7 J. Witte, P. Jordan and T. Turek, *Electrochim. Acta*, 2025, **517**, 145539.
8 C. Hank, A. Sternberg, N. Köppel, M. Holst, T. Smolinka, A. Schaadt, C. Hebling and H.-M. Henning, *Sustain. Energy Fuels*, 2020, **4**, 2256–2273.
9 M. R. Usman, *Renew. Sustain. Energy Rev.*, 2022, **167**, 112743.
10 K. Mazloomi and C. Gomes, *Renew. Sustain. Energy Rev.*, 2012, **16**, 3024–3033.
11 C. Chu, K. Wu, B. Luo, Q. Cao and H. Zhang, *Carbon Resour. Convers.*, 2023, **6**, 334–351.
12 M. Luberti and H. Ahn, *Int. J. Hydrogen Energy*, 2022, **47**, 10911–10933.

13 M. Rhandi, M. Trégaro, F. Druart, J. Deseure and M. Chatenet, *Chin. J. Catal.*, 2020, **41**, 756–769.
14 M. Trégaro, M. Rhandi, F. Druart, J. Deseure and M. Chatenet, *Chin. J. Catal.*, 2020, **41**, 770–782.
15 M. Chhetri, D. P. Leonard, S. Maurya, P. Sharan, Y. Kim, A. Kozhushner, L. Elbaz, N. Ghorbani, M. Rafiee, C. Kreller and Y. S. Kim, *Nat. Energy*, 2024, **9**, 1517–1528.
16 W. Xiao, H. Wang, A. Cheng, H. Wang, Z. Yang, X. Wu, X. Jiang and G. He, *Membranes*, 2023, **13**, 689.
17 A. Brouzgou, A. Seretis, S. Song, P. K. Shen and P. Tsiakaras, *Int. J. Hydrogen Energy*, 2021, **46**, 13865–13877.
18 S. Bai, C. Wang, M. Deng, M. Gong, Y. Bai, J. Jiang and Y. Xiong, *Angew. Chem., Int. Ed.*, 2014, **53**, 12120–12124.
19 E. G. Ciapina, S. F. Santos and E. R. Gonzalez, *J. Electroanal. Chem.*, 2018, **815**, 47–60.
20 S. Seidel, I. Kappel, C. Weidenthaler, P. J. Hausoul and R. Palkovits, *J. Catal.*, 2024, **438**, 115712.
21 C. Guan, D.-D. Zhang, Y. Pan, M. Iguchi, M. J. Ajitha, J. Hu, H. Li, C. Yao, M.-H. Huang, S. Min, J. Zheng, Y. Himeda, H. Kawanami and K.-W. Huang, *Inorg. Chem.*, 2017, **56**, 438–445.
22 B. Loges, A. Boddien, H. Junge and M. Beller, *Angew. Chem., Int. Ed.*, 2008, **47**, 3962–3965.
23 S. Kar, M. Rauch, G. Leitus, Y. Ben-David and D. Milstein, *Nat. Catal.*, 2021, **4**, 193–201.
24 G. Venugopalan, D. Bhattacharya, E. Andrews, L. Briceno-Mena, J. Romagnoli, J. Flake and C. G. Arges, *ACS Energy Lett.*, 2022, **7**, 1322–1329.
25 J. Zou, Y. Jin, Z. Wen, S. Xing, N. Han, K. Yao, Z. Zhao, M. Chen, J. Fan, H. Li and H. Wang, *J. Power Sources*, 2021, **484**, 229249.
26 M.-T. Nguyen, S. A. Grigoriev, A. A. Kalinnikov, A. A. Filippov, P. Millet and V. N. Fateev, *J. Appl. Electrochem.*, 2011, **41**, 1033–1042.
27 S. Mrusek, P. Preuster, K. Müller, A. Bösmann and P. Wasserscheid, *Int. J. Hydrogen Energy*, 2021, **46**, 15624–15634.
28 Q. Liu, S. Du, T. Liu, L. Gong, Y. Wu, J. Lin, P. Yang, G. Huang, M. Li, Y. Wu, Y. Zhou, Y. Li, L. Tao and S. Wang, *Angew. Chem., Int. Ed.*, 2024, **63**, e202315157.
29 Y. Wu, G. Huang, S. Du, M. Li, Q. Liu, Y. Zhou, Z. Jiang, X. Zhu, Y. Wang, T. Wang, L. Tao and S. Wang, *J. Am. Chem. Soc.*, 2024, **146**, 9657–9664.
30 Y. Wu, X. Zhu, S. Du, G. Huang, B. Zhou, Y. Lu, Y. Li, S. P. Jiang, L. Tao and S. Wang, *Proc. Natl. Acad. Sci. U. S. A.*, 2023, **120**, e2300625120.
31 A. Monshi, M. R. Foroughi and M. R. Monshi, *World J. Nano Sci. Eng.*, 2012, **2**, 154–160.
32 *Kratos Analytical Ltd*, ESCApe, version 1.5.1.1051, 2024.
33 N. Fairley, V. Fernandez, M. Richard-Plouet, C. Guillot-Deudon, J. Walton, E. Smith, D. Flahaut, M. Greiner, M. Biesinger, S. Tougaard, D. Morgan and J. Baltrusaitis, *Appl. Surf. Sci. Adv.*, 2021, **5**, 100112.
34 M. C. Biesinger, *Appl. Surf. Sci.*, 2022, **597**, 153681.
35 L. Yao, J. Gu, W. Wang, T. Li, D. Ma, Q. Liu, W. Zhang, W. Abbas, A. Bahadoran and D. Zhang, *Nanoscale*, 2019, **11**, 2138–2142.
36 H. Junge, A. Boddien, F. Capitta, B. Loges, J. R. Noyes, S. Gladiali and M. Beller, *Tetrahedron Lett.*, 2009, 1603–1606.
37 K. V. A. Birkelbach, H. Hartmann, A. Besmehn, A. Meledin, I. Kappel, P. J. C. Hausoul and R. Palkovits, *EES Catal.*, 2025, **3**, 701–711.
38 P. V. Snytnikov, M. M. Zyryanova and V. A. Sobyanin, *Top. Catal.*, 2016, **59**, 1394–1412.
39 L. P. Bakos, M. Bohus and I. M. Szilágyi, *Molecules*, 2023, **28**, 4344.
40 K. H. Hong, G. M. McNally, M. Coduri and J. P. Attfield, *Z. Anorg. Allg. Chem.*, 2016, **642**, 1355–1358.
41 P. Rheinländer, S. Henning, J. Herranz and H. A. Gasteiger, *ECS Trans.*, 2013, **50**, 2163–2174.
42 W. Sheng, *J. Electrochem. Soc.*, 2010, **157**, 1529–1536.
43 A. V. Tripkovic, *J. Serb. Chem. Soc.*, 2003, **68**, 849–857.
44 P.-A. Carlsson, V. P. Zhdanov and M. Skoglundh, *Phys. Chem. Chem. Phys.*, 2006, **8**, 2703–2706.
45 D. Levitan, A. Rozenblit, M. Laborde and P. Giunta, *J. Electroanal. Chem.*, 2021, **880**, 114924.
46 K. G. Nishanth, P. Sridhar and S. Pitchumani, *Int. J. Hydrogen Energy*, 2013, **38**, 612–619.
47 K. Kwon, Y. Jung, H. Ku, K. H. Lee, S. Kim, J. Sohn and C. Pak, *Catalysts*, 2016, **6**, 68.

